Published in final edited form as:
Am J Physiol. 1992 February ; 262(2 0 2): H420–H431.

Capillary endothelial transport of uric acid in guinea pig heart

KEITH KROLL, **THOMAS R. BUKOWSKI**, **LISA M. SCHWARTZ**, **DAVID KNOEPFLER**, and **JAMES B. BASSINGTHWAIGHTE**
Center for Bioengineering, University of Washington, Seattle, Washington 98195

Abstract

Much of the adenosine formed in the heart is degraded by endothelial enzymes to uric acid, which is exported across the coronary capillary endothelial cell membrane before renal excretion. Because previous experiments suggested that cell permeability for uric acid is either very high (similar to water) or very low, multiple indicator-dilution experiments were carried out to distinguish between the two possibilities. An intravascular reference tracer, ^{l31}I-labeled albumin, and an extracellular reference tracer, L-[^{3}H]glucose, were injected together with [^{14}C]uric acid as a bolus into the coronary inflow, while fractionating the venous outflow for 90 s. Recovery of injected uric acid averaged 99.0 ± 2.9% (mean ± SD, n = 12) that of L-glucose. Peak capillary extraction of Multiple tracer dilution estimates of L-glucose and uric acid averaged 0.38 ± 0.032 and 0.42 ± 0.035 ($P < 0.005$) compared with albumin. Except at the peaks, the dilution curves for [^{14}C]-uric acid and L-[^{3}H]glucose coincided closely, indicating that little uric acid was transported into cells. The dilution curves were analyzed using an axially distributed, multipathway, four region mathematical model, to estimate membrane permeability-surface area (*PS*) products. Since the endothelial cell *PS* for uric acid was low (0.12 ± 0.09 ml·g^{-1}·min^{-1}), ~3% of the *PS* reported for adenosine, the possibility of flow-limited exchange for uric acid is ruled out. To estimate steady-state endothelial concentrations of uric acid in vivo, equations were developed describing electrochemical potential gradients for dissociated and undissociated forms of a weak acid. Despite endothelial production, intracellular concentrations that are lower than outside are expected because the negative membrane potential and lower cellular pH assist uric acid efflux.

Keywords

urate; capillary permeability; adenosine; microvascular; weak acid; multiple-indicator dilution; coronary; nucleoside transport; purines

---

CONSTANT TURNOVER of adenine nucleotides in the heart results in the continuous cellular production of adenosine via the hydrolysis of 5′-AMP. In addition to direct rephosphorylation, adenosine is subject to enzymatic degradation to inosine, hypoxanthine, xanthine, and finally uric acid. Although some hypoxanthine can be salvaged, this catabolic sequence results in a net loss of myocardial purines of ~2 nmol·min^{-1}·g^{-1} (12), representing a drain on the total myocardial adenine nucleotide pool of 2%/h. This purine loss occurs mostly via the coronary efflux of uric acid (12) formed by the enzyme xanthine oxidase/dehydrogenase, which is largely confined to capillary endothelial cells (20). Therefore most uric acid formed in the heart must be transported across the cell membrane of the capillary

endothelium before renal excretion or hepatic metabolism to allantoin in species possessing the enzyme uricase.

Coronary endothelial transport of adenosine occurs via facilitated diffusion, mediated by a membrane nucleoside carrier with a moderately high permeability-surface area (*PS*) product for endothelial cells (31). Although the normal coronary efflux of uric acid in the guinea pig is ~15-fold greater than that of adenosine (2), coronary endothelial permeability for uric acid is unknown. If endothelial *PS* were low, then the observed rates of coronary efflux of uric acid might involve relatively high concentrations of uric acid in endothelial cytoplasm compared with plasma concentrations. On the other hand, low intracellular pH and a negative membrane potential might assist in the efflux of uric acid, resulting in low intracellular concentrations. Elevated endothelial concentrations would increase the possible role of uric acid as an antioxidant and radical scavenger (13). Radical scavenging may be relevant to the role of uric acid formation in the generation of oxygen free radicals, which occurs if xanthine dehydrogenase is converted to its oxidase form. In addition, elevated endothelial uric acid might exert product inhibition over xanthine oxidase/dehydrogenase if its concentration approached 200 μM, the inhibition constant (K_i) for uric acid in vitro (16). Decreased hypoxanthine oxidation caused by elevated uric acid would most likely increase the competing pathway leading to incorporation of hypoxanthine into myocardial adenine nucleotides, representing a role in the regulation of the purine salvage pathway.

The background to the present study was preliminary results showing the time course of labeled uric acid in the coronary venous effluent after the injection of tracer adenosine into the arterial inflow of the isolated guinea pig heart (Fig. 1). The injected adenosine was metabolized in the heart, giving rise to the efflux curves of labeled inosine, hypoxanthine, xanthine, and uric acid via action by the enzymes adenosine deaminase, purine nucleoside phosphorylase, and xanthine oxidase/dehydrogenase, respectively. Inosine emerged with nearly the same time course as that of precursor adenosine, and the outflow of hypoxanthine and xanthine were low, near the methodological detection limit. However, the efflux of uric acid was greater than that of the other metabolites and exhibited a marked delay. The delay has two possible explanations, based on an analysis using an extension of the multiple metabolite model described by Catravas and co-workers (14). One explanation was that the cellular efflux of uric acid was impeded by a low membrane *PS* product. The other possible explanation was that the endothelial and parenchymal cell membrane *PS*s for uric acid were very high, resulting in flow-limited washout from a volume of distribution equal to that of water. The present study was carried out to resolve this uncertainty.

The multiple indicator-dilution method was employed because it provides the needed high temporal resolution and is particularly sensitive to capillary endothelial transport. This technique relied on the efflux kinetics of an intravascular reference tracer ^{131}I-albumin and an extracellular reference tracer L-[^{3}H]glucose to define the transport of small hydrophilic solutes through the interendothelial clefts between the vascular and interstitial regions of the heart. L-Glucose was used as an extracellular reference because its membrane transport is negligible during the brief period of an indicator dilution curve (22, 24). Capillary endothelial and parenchymal cell membrane permeabilities for uric acid were assessed by analyzing the differences between the dilution curves of L-[^{3}H]glucose and [^{14}C]uric acid.

For the analysis, a physically realistic, multiple capillary, four-region, axially distributed model of blood-tissue exchange processes (10) was used. If *PS* were quite low, then dilution curves of uric acid and L-glucose should be similar. If *PS* were quite high, then the two dilution curves should deviate markedly, uric acid transport approaching a flow-limited condition (5).

The results obtained indicate that capillary endothelial membrane *PS* for uric acid was very low, ~3% of the endothelial *PS* reported for adenosine in the same preparation (31). To estimate physiological concentrations of free uric acid within endothelial cells using these results, it is necessary to account for the additional effects of intracellular pH and membrane potential on a weak acid, which is produced intracellularly. To analyze this problem, a model that describes membrane transport of both the dissociated and undissociated forms of a weak acid was developed. Despite the endothelial production of uric acid and the low membrane *PS*, it is predicted that steady-state uric acid concentrations in vivo are normally lower inside endothelial cells than outside.

METHODS

Triple-Label and Dual-Label Studies

Studies were carried out in a total of six isolated, nonworking perfused hearts of guinea pigs, a species in which coronary endothelial cells are active in purine metabolism (27). In each heart, three multiple indicator-dilution experiments were carried out, for a total of 18 indicator-dilution studies.

Triple-label studies—In four hearts, [^{14}C]uric acid and vascular and extracellular reference tracers ^{131}I-albumin and L-[^{3}H] glucose were used, respectively.

Dual-Label studies—In two hearts, [^{14}C]uric acid and L-[^{3}H]glucose alone were used to decrease the nontracer concentration of uric acid in the tracer injectate by 50-fold compared with the triple-label studies. The dual-label study was necessary to demonstrate clearly the endothelial uptake of uric acid, which was near the detection limit of the multiple indicator-dilution technique.

Heart Preparation

The hearts of six heparinized (300 U), anesthetized (pentobarbital sodium, 50 mg/kg) adult guinea pigs were rapidly excised and placed on Langendorff perfusion using oxygenated (95% O_2-5% CO_2), filtered (1.2 μm) modified Krebs-Ringer bicarbonate buffer of the following composition (concentrations in mM): 143 Na, 5.0 K, 2.1 Ca, 0.7 Mg, 126 Cl, 25 $HC0_3$, 1.2 H_2P0_4, 0.7 SO_4, 0.1 EDTA, and 5 glucose and 0.1% bovine serum albumin (US Biochemical, fraction V) at pH 7.4 and 37°C. A peristaltic pump directed perfusate from a reservoir through a temperature-controlled (37°C) windkessel to the heart. The flow rate (averaging 8.6 ± 3.6 ml/min, equivalent to 3.5 ± 0.6 ml·g^{-1}·min^{-1}, mean ± SD, n = 18) was adjusted to provide a perfusion pressure of 50–80 mmHg, which was recorded throughout the experiment. After the pulmonary artery and the caval entries of the right atrium were ligated, coronary effluent perfusate was directed from the right ventricle via a narrow

polyethylene cannula passing through the ventricular wall to a motor-driven rotating sampler system. The left ventricle was drained by a small cannula inserted through the apex of the heart. A second perfusate reservoir was filled with medium containing 1 mM uric acid, which was otherwise identical with the normal medium. The perfusion system was arranged to switch rapidly from one perfusion medium to the other, avoiding perfusate stagnation by continuous recirculation of the medium not in use for perfusion. The dead volume of the perfusion cannula and valve system (0.37 ml) was replaced ~30 times in 60 s. Hearts were electrically paced at 300 beats/min.

Protocol for Triple-Label Studies

Hearts of four animals were perfused for ~15 min with normal medium after preparation described above. The first tracer bolus (~0.1 ml) was injected into the inflow of the aortic cannula during perfusion with normal medium. At the same time, the coronary effluent perfusate was fractionated by the knife edges of the rotating samplers at 1-s intervals for 30 s and at 2-s intervals for the next 60 s. Perfusate fractions were collected directly into preweighed glass liquid scintillation minivials that were reweighed to quantify each collected fraction. Before and after the tracer injection, coronary outflow through the right ventricular cannula was measured using a graduated cylinder and stopwatch. Approximately 15 min after the first tracer injection, the perfusate was switched to one containing 1 mM uric acid, and 60 s later a second tracer bolus was injected while the outflow was fractionated as before. This experiment was designed to test for possible competitive inhibition of cold uric acid with tracer uric acid. Flow through the outflow cannula was measured after collection of effluent samples after which perfusion was restored to the normal medium. After 15 min perfusion with normal medium, the final tracer injection was made, with fractions collected as before. Altogether, 12 multiple indicator-dilution experiments were performed in the triple-label studies. Approximately 1 μCi of 15 μm-diam radioactive microspheres (^{85}Sr or ^{131}Sn, New England Nuclear) was injected into the arterial inflow of the heart to determine the regional distribution of coronary flow. The heart was removed from the perfusion cannula, trimmed of fat and connective tissue, weighed, and frozen until sectioning for determination of microsphere deposition. The syringes containing the tracer bolus were weighed empty before and after each injection. The injectate remaining in the syringe after each injection was diluted into 1.0 ml perfusate, aliquots of which were analyzed to quantify the tracer injected.

Protocol for Dual-Label Studies

Because the specific activity of [^{14}C]uric acid used was relatively low (8 mCi/mmol), the chemical concentration of uric acid in the effluent perfusate resulting from the tracer injection averaged 5 μM at the peak of the outflow dilution curves in the triple-label studies. To decrease the concentration of uric acid, six additional experiments were carried out using two hearts in which the injectate content of [^{14}C]uric acid was decreased to ~2% of that used in the triple-label studies. To minimize error in the determination of ^{14}C activity, ^{131}I-labeled albumin was omitted from the injectate and the content of L-[^{3}H]glucose was decreased to ~5% of its previous level. The experimental protocol was the same as in the triple-label studies except the effluent perfusate was sampled at 1-s intervals for 20 s.

Tracers

^{131}I-labeled albumin (half-life 8.1 days) was used as the intravascular reference tracer. Bovine serum albumin (fatty acid free) was radioiodinated using the chloramine-T technique (25) and was fractionated on a Sephadex G-25 liquid chromatographic column, using a buffer solution consisting of 0.05 M KH_2P0_4 (pH 7.0) to remove free ^{131}I. Before each experiment, the albumin fraction was dialyzed overnight at 20°C against 1 liter of perfusion medium and vacuum filtered (0.2 μm) to remove any aggregated albumin particles. L-[1-^{3}H(N)]glucose (sp act 20 Ci/mmol, New England Nuclear), used as the extracellular reference tracer, was evaporated to dryness and dissolved in perfusion medium on the day of each experiment. [2^{14}C]uric acid (sp act 2 mCi/mmol, California Bionuclear) was purified by high-pressure liquid chromatography (HPLC) before each experiment, increasing its specific activity to ~8 mCi/mmol. The tracer injectate was prepared by pooling the three tracers in aliquots of the same perfusion medium used at the time of each bolus injection. Each tracer bolus contained 0.3 μCi ^{131}I-labeled albumin, 0.4 μCi L-[^{3}H]glucose, and 0.07 μCi [^{14}C]uric acid. Tracer solutions were centrifuged (5 min, 10,000 g) before injection.

Radioisotope Counting

In the triple-label group, activity in the weighed effluent perfusate fractions was determined by three-channel liquid scintillation β counting using a gel-phase system. Aliquots of the diluted injectate were also counted to quantify the tracer dose injected. Scintillation cocktail (RediSolv MP, 3.6 ml) and picric acid (saturated solution, diluted 1:8,000, 2.3 ml) were added to the samples, and the glass vials were shaken vigorously to produce an evenly dispersed gel before counting on a Beckman Instruments LS 5801 for 30 min. A gel phase was necessary to prevent spectral instability of ^{131}I-albumin in the scintillation medium. Quench and spectral spillover corrections were made by a matrix inversion method based on a Gaussian elimination technique using results obtained from four series of quench standards (background, ^{131}I, ^{3}H,^{14}C) fitted by least-squares polynomials. In the dual-label studies, sample activity was determined by two-channel beta counting for 60 min using a liquid-phase system and appropriate quench standards.

To determine regional microsphere deposition, four hearts were sectioned into four rings, each ring into eight sectors, and each sector into endocardial and epicardial halves. Each piece was weighed and counted for gamma activity in a multichannel well counter.

Calculation of Dilution Curves

Normalized dilution curves, or the "transport function" *h(t)*, were calculated from the expression, $h(t) = F' C(t)/q_o$, where *h(t)* is the fraction of injected tracer emerging in the coronary outflow per second (having units, s^{-1}), F' is the flow of perfusate (in ml/s) measured at the time of each dilution curve, C(*t*) is the tracer activity in the effluent fraction (dpm/ml) at time *t*, and q_o is the tracer activity (dpm) injected in the bolus. The instantaneous fractional extraction of L-glucose and uric acid, E(*t*), was calculated from the expression, $E(t) = 1 - h_D(t)/h_R(t)$, where $h_D(t)$ is the transport function for L-glucose or uric acid and $h_R(t)$ is that for albumin, assuming that ^{131}I–albumin did not leave the intravascular space. Peak extraction, E_{max} was E(*t*) at the peak of the albumin curve.

Modeling Analysis

Overview—The multiple indicator-dilution curves were analyzed usi ng a four-region, multicapillary, axially distributed model of microvascular transport and exchange. The methods for using such models have been presented by Bassingthwaighte and Goresky (5) and by Kuikka and co-workers (22). To account for the effects of the spatial heterogeneity of coronary flow (21), the present model consisted of 20 parallel vascular pathways identical except for their flows, each consisting of a nonexchanging vessel unit and a capillary-tissue exchange unit. In each capillary-tissue unit, vascular, endothelial cell, interstitial, and parenchymal cell regions were represented (Fig. 2). The model is the same as that described previously (10, 31), except that previous models used only five pathways to represent flow heterogeneity and did not include a nonexchanging vessel in each flow pathway.

Flow heterogeneity—The distributions of regional flows in the guinea pig hearts were similar to those found by Gorman and co-workers (19). They were broadened to a relative dispersion of 55% to account for the heterogeneity closer to that at the capillary level (9) and were represented by a lagged normal density function using 20 discrete flows for the pathways in the model.

To account for both the dispersion and delay due to transport through medium-sized nonexchanging arteries and veins, an operator was included in series with each capillary tissue unit composed of a pure delay line in series with a dispersive fourthorder differential operator (2 2nd-order operators in series). The parameters used for the fourth-order operator yielded a relative dispersion (coefficient of variation of the impulse response) of 48% (7). By setting the delay operator to provide 60% of the total mean transit time of the medium vessel operator, the relative dispersion of the composite vessel operator was constrained to equal the dispersion found in arteries (3), since 0.48 × (1.0 − 0.6) = 0.192. Because the operator accounts for both arterial and venous dispersion (convolution being commutative), we assume equal dispersion in the two vessel segments. Pathways were assigned the same medium vessel volume, 0.08 ml/g, regardless of flow, so that pathway transit times were inversely proportional to the pathway flows. A common trunk vessel feeding and draining the set of individual pathways is accounted for in the deconvolution. The dispersive nature of the medium vessel operator is more realistic than the pure delay lines used by Rose and Goresky (28) and accounts for the expected association between medium-sized vessels and capillary transit times.

Model parameters—The parameters controlling transport, exchange, and metabolic processes for tracers are described below. Because L-glucose was used as an extracellular reference, the only parameters used to fit the L-glucose dilution curve were PS_g, and V'_{isf}. To fit the uric acid curve, only PS_{eC1} and PS_{eca} were adjusted; all other parameters were given fixed values (see below, *Reduction of degrees of freedom*).

F_P Perfusate flow (measured)

PS_g *PS* product for extracellular exchange between vascular and interstitial regions via interendothelial clefts (determined by fitting L-glucose curve)

P_{ecl} Luminal membrane *PS* product for endothelial cells (adjusted to fit uric acid curve)

P_{eca} Abluminal membrane *PS* product for endothelial cells (adjusted to fit uric acid curve)

PS_{pc} Membrane *ps* product for parenchymal cells (fixed at 0)

V_p Intracapillary volume (fixed at 0.035 ml/g)

V'_{ec} Endothelial cell volume of distribution (fixed at 0.03 ml/d Interstitial

V'_{isf} Interstitial fluid volume of distribution (determined by fitting L-glucose curve)

V'_{pc} Parenchymal cell volume of distribution (fixed at 0.55 ml/d Consumption

G_{ec} Consumption (clearance) in endothelial cells (fixed at 0)

G_{pc} Consumption (clearance) in parenchymal cells (fixed at 0)

Units for parameters *PS*, F_p, and G are milliliters per minute per gram. These parameters are constants, independent of tracer concentrations.

Modeling strategy—For the triple-label studies, the initial step in the modeling was to obtain an input function for all three tracers. This was obtained by deconvolving the albumin-dilution curve with the overall model transport function for the intravascular reference tracer. The overall transport function is the model impulse response, which is explicitly determined by the model characteristics.

The second stage of analysis was to obtain estimates of the parameters governing extracellular transport, PS_g, and V'_{isf}. This was carried out by adjusting these parameters to optimize the model fit to the first 30 s of the L-glucose-dilution curve using the input function obtained by deconvolution.

The final stage was to model the dilution curve for uric acid. Because PS_g, represents transport by diffusion, the parameter value for uric acid was obtained by multiplying the value found for L-glucose by 1.04, the reciprocal of the square root of the ratio of molecular weights (168/182) (30). No correction was applied to V'_{isf}, since the volume exclusion of uric acid in the interstitial fluid region was calculated to be only 0.04% less than for glucose using the approach of Schafer and Johnson (29). Permeation of uric acid into endothelial cells was modeled by adjusting PS_{ecl} and PS_{eca} (for the luminal and abluminal surfaces) to improve the model fit using an automated nonlinear least-squares optimizer routine (4).

Estimates of endothelial permeability were determined almost entirely by fitting the curve peak, based on sensitivity-function analysis (10). In 11 of the 12 data sets, the optimized value of PS_{pc} was constrained to zero, the adjustment of a single parameter, PS_{ecl}, determined the fit of the model to the uric acid data. This represents an overdetermined condition, since at least three data points in every curve constrain this parameter.

For the dual-label studies, the input function was modeled by a lagged normal density function, the shape of which was adjusted, so that the L-glucose model solution gave a close fit to the L-glucose curve using the average values of PS_g and V'_{isf} obtained in the triple-label studies. The parameters PS_{ecl} and PS_{eca} were then adjusted to fit the entire uric acid curve as described above. Any small errors in this method of obtaining an input function only affect the later portions of the curve and do not influence the estimates of endothelial permeability, because the data sets were relatively short (20 s).

Reduction of degrees of freedom—Because the greatest accuracy in parameter estimation is achieved when the degrees of freedom are minimal, several parameters were given constant values for all experiments where this was appropriate. For L-glucose, all membrane PS_s were given values of zero (definition of extracellular reference). V_p and V'_{ec} were given values of 0.035 (11) and 0.030 (1) ml/g, respectively, based on anatomic data. Endothelial consumption G_{ec} was given a value of zero based on the assumption that metabolism of uric acid in the heart was negligible: total recovery of uric acid was within 1% that of L-glucose (see RESULTS), and uricase activity is largely confined to the liver (17). Parenchymal cell permeability PS_{pc} was given a value of zero, since the close similarity in the later portions of the dilution curves of uric acid and L-glucose provided no evidence for parenchymal cell permeation. This eliminated any role for G_{pc} and V'_{pc} in the modeling. Coronary flow F_p, was measured directly in each experiment, and the same distribution of flows was used in the modeling analysis of all the dilution curves. Altogether, this left two degrees of freedom for fitting the L-glucose curves and two (in practice, only one) for fitting the uric acid curves.

RESULTS

Flow Heterogeneity

In the four hearts in which the regional heterogeneity of coronary flow was measured using tracer microspheres, tissue pieces with a mean weight of 39 mg (n = 217) had an average relative dispersion (SD/mean) of flows of 0.31. The fractal relationship describing the spatial heterogeneity of coronary flow (6) predicts that the relative dispersion increases as the tissue is divided into smaller pieces, because of spatial averaging within the tissue pieces analyzed. Therefore 31% underestimates the degree of heterogeneity at the level of capillarytissue units, which is most likely governed at the level of terminal arteriolar units, ~100 μg. If the curved fractal relationship between volume element size and relative dispersion for a branching arterial network (9) is assumed, the functional value for relative dispersion at the level of the microvascular exchange unit is ~55%. This value was used to define the distribution of flows through the 20 pathways of the model in an attempt to avoid

the systematic underestimation of PS_s that occurs when heterogeneity is not accounted for (5).

Triple-Label Multiple Indicator-Dilution Studies

Tracer-dilution curves—Typical multiple indicator-dilution curves for ^{131}I-albumin, L-[^{3}H]glucose, and [^{14}C]-uric acid are shown in Fig. 3. In Fig. 3A a linear ordinate was used for *h(t)* and only the early parts of the curves are plotted so as to present the peaks clearly. In Fig. 3B a logarithmic ordinate was used for *h(t)* and the entire dilution curves are shown. The albumin curve has a higher peak and a more rapid decline than the curves for L-glucose and uric acid, since these much smaller solutes cross the capillary wall and have a larger volume of distribution than albumin. At the peak, the uric acid curve was lower than that of the extracellular reference, L-glucose, although later the L-glucose and uric acid curves coincided closely. E_{max} of uric acid, 0.419 ± 0.035 (mean ± SD, n = 12), was greater than that of L-glucose, 0.384 ± 0.032, in all 12 experiments (Table 1), averaging an 8.4% difference ($P < 0.005$, paired comparison). Total outflow recovery of the uric acid injected in the tracer bolus averaged 99.0 ± 2.9% of the recovery of L-glucose, indicating negligible retention of uric acid beyond 90 s.

Modeling L-glucose curves—To obtain estimates for the parameters describing extracellular transport, PS_g and V'_{isf} the model was fitted to the first 30 s of the dilution curves of L-glucose (Table 2).

Modeling uric acid curves—The next step was to compare fits to uric acid-dilution curves obtained using models excluding and including membrane transport. Figure 4 shows a typical dilution curve fit by model solutions for albumin, L-glucose, and uric acid. Only the first 15 s of the curve are given so as to show the peak clearly, where the effects of PS_{ecl} are greatest. The solution excluding membrane transport for uric acid (Fig. 4, dashed line) was obtained by constraining PS_{ecl}, PS_{eca} and PS_{pc} to equal zero. This solution shows slightly greater extraction than that of the L-glucose solution (dotted line), because PS_g, was corrected for the difference in molecular weights between uric acid and L-glucose (see METHODS, *Modeling strategy*). The solution including membrane transport based on an optimized value of PS_{ecl} of 0.20 ml·g^{-1}·min^{-1} (dash-dot line) fits the data better at the peak of the curve, where sensitivity to PPS_{ecl} is greatest. In this experiment, accounting for endothelial permeability decreased the coefficient of variation of the fit (SD/mean) by 22% compared with the solution obtained when $PS_{ecl} = 0$. Except for PS_{ecl}, all other model parameters were identical for the two uric acid solutions In 8 of the 12 experiments in the triplelabel studies, the coefficient of variation was decreased by nonzero values for PS_{ecl} (Table 3). The average value of PS_{ecl} giving the best fit in all 12 experiments in four hearts was 0.12 ± 0.09 ml. g^{-1}. min^{-1}, which decreased the coefficient of variation by an average 14% compared with fits with $PS_{ecl} = 0$. Significantly better model fits ($P < 0.005$) were obtained using the optimized values of PS_{sel} compared with fits based on fixed values of PS_{ecl} equal to 0, 0.2, and 0.3 ml·g^{-1}·min^{-1} (Table 3). Because of low sensitivity for PS_{eca} it was not possible to obtain reliable nonzero estimates for abluminal permeability by parameter optimization. However, the uncertainty in PS_{eca} had little effect on estimates of PS_{ecl}.

The individual differences between peak extractions of uric acid and L-glucose are shown in Fig. 5A at the coronary flow rates determined in each experiment (solid circles). In addition, the flow dependence of the differences between peak extractions predicted by the model (continuous curves) are shown for five values of PS_{ecl} between 0 and 0.24 $ml \cdot g^{-1} \cdot min^{-1}$, keeping all other model parameters unchanged. The solution for $PS_{ecl} = 0$ shows excess extraction of uric acid over L-glucose, because of the correction for the difference between the molecular weights of uric acid and L-glucose. This analysis of the single samples obtained at the peak of each dilution curve suggests a higher value for PS_{ecl} (~0.24 $ml \cdot g^{-1} \cdot min^{-1}$) than the value of 0.12 $ml \cdot g^{-1} \cdot min^{-1}$ obtained above based on analysis of the entire curve peak (O–30 s). This apparent inconsistency is clarified in Fig.5B, where the differences between the instantaneous extractions of uric acid and L-glucose are shown for the points 1 s before the peak of the curve, the points at the peak ($t = t_{peak}$), and the points 1 s after the peak. The points before and after the peak show less excess extraction of uric acid than the points at the peak of the curve (the individual data for which are shown in Fig. 5A). In addition, model solutions shown were obtained using the same values of PS_{ecl} as in Fig. 5A at a flow rate of 3.3$ml \cdot g^{-1} \cdot min^{-1}$, the average experimental value.

Parenchymal cell permeability—The close coincidence of the late portions of the L-glucose- and uric acid-dilution curves (Fig. 3) indicated that PS_{pc} for uric acid was small but not zero. If PS_{pc} had been larger, the uric acid curve would have been lower than the L-glucose curve in the time interval 15–30 s after injection because of retention in parenchymal cells. If PS_{pc} had been zero, the uric acid curve would have exceeded the L-glucose curve at later times after injection because of reflux from late interstitial region. Because of the similarity in the late portions of the curves, PS_{pc} was estimated to 0.010 $ml \cdot g^{-1} \cdot min^{-1}$ based on analysis of the time interval t = 70–90 s, where model sensitivity for this parameter is greatest (10). This small value of PS_{pc} has no influence on the modeling estimates of endothelial permeability.

Uric acid—The presence of 1 mM uric acid in the perfusion medium had no consistent effect on estimates of PS_{ecl} (Table 3). These experiments were conducted in an effort to assess competitive inhibition of endothelial uptake of [^{14}C]uric acid by 1 mM unlabeled uric acid. Competitive inhibition, expected for a saturable membrane carrier, would have abolished the difference in E_{max} between L-glucose and uric acid. However, because this difference was near the detection limit in the absence of 1 mM uric acid, the failure to detect a decrease provides no ev idence against a specific membrane carrier for uric acid.

Dual-Label Multiple Indicator-Dilution Studies

One possible explanation for the low endothelial permeability for uric acid observed in the triple-label studies is that a high-affinity transporter was competitively inhibited by the relatively high nontracer levels of uric acid in the tracer injectate (see METHODS, *Protocol for Dual-Label Studies*). This possibility was ruled out by separate experiments in which the injectate concentration of uric acid was decreased to ~2% of that in the triple-label studies. If saturation of a carrier had been problem in the triple-label studies, then PS_{ecl} would have been higher in the dual-label studies. However, estimates of PS_{ecl} in the dual-label studies (0.051 ± 0.037 $ml \cdot g^{-1} \cdot min^{-1}$, n = 6; Table 3) were not higher than in the triplelabel studies

(0.12 ± 0.09 ml·g^{-1}·min^{-1}). As in the triplelabel studies, there was no consistent effect of 1 mM uric acid in the perfusion medium, and nonzero values for PS_{eca} could not be reliably estimated. Coronary flow averaged 3.9 ± 0.3 ml·g^{-1}·min^{-1} in the dual-label studies.

DISCUSSION

Analysis of the results presented in Fig. 1 using the methods described by Bassingthwaighte et al. (8, 10) suggested that membrane *PS* for uric acid was either so high that uric acid transport was flow limited (*PS* > 30 ml·g^{-1}·min^{-1}) or else that *PS* was very low. The present study was carried out to distinguish between these possibilities. The major finding of the present study is that the dilution curves of uric acid and the extracellular reference L-glucose show consistent evidence of a low endothelial transport of uric acid. The possibility of a high *PS* can be excluded, since it would result in markedly greater peak extraction of uric acid compared with that of L-glucose.

Accuracy of Estimates of Membrane PS

Although it is clear that uric acid exchange is not flow limited, the close similarity in the dilution curves of L-glucose and uric acid limited the accuracy of the estimates of endothelial cell *PS* (PS_{ecl}). As shown in Fig. 4, the differences between the dilution curves of L-glucose and uric acid were greatest at the peak of the curves, where the sensitivity for PS_{ecl} is greatest (10). The greater the difference between peak extractions, the greater was the resolution for estimating PS_{ecl}. The modeling results shown in Fig. 5 indicate that the expected differences in peak extractions are greatest for a given value of PS_{ecl} at a coronary flow rate of ~1.4 ml·g^{-1}·min^{-1}. Although extraction itself, E(t), must increase to a maximum of 1.0 as flow approaches zero, the difference between two similar extraction curves goes to zero. Therefore, if the flow rate in the present study had been decreased by 50%, the experimental sensitivity for estimating PS_{ecl} would have been ~20% greater than at the flow rate used. However, coronary perfusion at such a low rate with a medium devoid of erythrocytes would impair oxygen delivery.

The results of the present experiments provided evidence that parenchymal cell *PS* is lower than endothelial cell *PS*. A value of PS_{pc} as large as that estimated for PS_{ecl} would have caused measurable decreases in the uric acid curve compared with the L-glucose curve in the time interval 15–30 s after the injection. Although PS_{pc} was clearly less than PS_{ecl}, the similarity in the two curves introduces a level of uncertainty in distinguishing PS_{pc} from zero.

Decreasing the chemical content of uric acid in the tracer injectate in the dual-label studies did not increase estimates of PS_{ecl} compared with those in the triple-label studies. This finding tends to rule out the possibility that a possible uric acid transporter was saturated by the chemical content of uric acid in the tracer injectate. Only if the Michaelis constant (K_m) of such a transporter were below ~10 nM is it possible that the transporter would have been saturated in the dual-label studies. Because plasma concentrations of uric acid are at least 1,000-fold higher in mammals, such high affinity is unlikely.

Significantly better model fits to the uric acid dilution curves were obtained using the optimized values of PS_{ecl} for each experiment compared with fits obtained using fixed values of PS_{ecl} equal to 0, 0.2 and 0.3 ml·g^{-1}·min^{-1} (Table 3). Because the optimized values of PS_{ecl} (mean = 0.12 ml·g^{-1}·min^{-1}) could be distinguished from values of 0 and 0.2, it may be concluded that the true value endothelial permeability lies within the range $0 < PS_{ecl} < 0.2$ ml·g^{-1}·min^{-1} For comparison, PS_{ecl} for adenosine was estimated to be 4.6 ml·g^{-1}·min^{-1} under similar experimental conditions using the multiple indicator-dilution technique in the same preparation (31).

Advantages of the multiple pathway, multiple region model used to analyze the dilution curves are that accounts approximately for 1) differences in extracellular capillary *PS* (PS_g) in different hearts, 2) the effect the expanded interstitial volume of distribution present in the hearts studied, 3) different flow rates in individual hearts, and 4) regional flow heterogeneity. In addition, the effects of random methodological errors in individual outflow samples are reduced, since they tend to cancel out when multiple samples are analyzed. The major limitation in the modeling analysis was that membrane *PS* for uric acid was near the resolution of the multiple indicator-dilution technique. Greater sensitivity for estimating PS_{ecl} may be obtained from another type of experiment in which labeled uric acid is produced within capillary endothelial cells from tracer precursors, in Fig. 1. A second limitation was that the molecular weights of uric acid and L-glucose were not identical but differed by 8%. Although this effect should cause excess extraction of uric acid over L-glucose, the size of the effect is expected to be too small to detect.

Effects of Cellular pH and Membrane Potential on Steady-State Endothelial Uric Acid Concentrations

Based on the finding of the present study that the membrane *PS* for uric acid (PS_{ecl}) is low, it might supposed that physiological concentrations of free uric acid within endothelial cells are considerably higher than extracellular levels because uric acid is mostly produced within endothelial cells (20). However, cellular concentrations depend on the membrane electrochemical potential gradients, which are quite different for the dissociated and undissociated forms of a weak acid. To account for the effects of intracellular pH and membrane potential, we developed a general model (see APPENDIX) describing separate membrane transport mechanisms for dissociated and undissociated forms of uric acid. The analysis predicts that steady-state concentrations of free uric acid are normally lower inside endothelial cells than outside, because the pH gradient and membrane potential assist efflux.

The steady-state expression (Eq. A11 of APPENDIX) gives the intracellular concentration of the total uric acid ($[U_t]_i$), dissociated plus undissociated forms, in terms of the total extracellular concentration ($[U_t]_o$, the dissociation constant (K_a, M), the membrane potential (E_m, mV), the permeabilities (P^D and P^U, cm/s) of the dissociated and undissociated forms, and the production (Y, mol·g^{-1}.s^{-1})

$$[U_t]_i = \frac{(K_a + [H^+]_i)\left\{\frac{[U_t]_o K_a}{K_a + [H^+]_o}([H^+]_o - \alpha K_a) + \frac{Y K_a}{P^U S}\right\}}{K_a([H^+]_o - \alpha K_a e^{E_m zF/RT})}$$

where S is membrane surface area (cm^2/g); valence z, Faraday F, universal gas constant R, and absolute temperature T have their usual meanings and units; and α is a dimensionless constant dependent on the membrane potential and the ratio of the permeabilities

$$\alpha = \frac{P^{D}S}{P^{U}S} \frac{E_m z f}{RT\left(1 - e^{E_m z f/RT}\right)}$$

Figure 6 shows the predicted ratio of intracellular to extracellular free concentrations, $[U_t]_i/[U_t]_o$, as a function of the ratio of the permeabilities of the dissociated to undissociated forms, P^D/P^U. The five curves represent solutions obtained for five values of endothelial uric acid production between 0 and 10 $nmol \cdot g^{-1} \cdot min^{-1}$. The concentration weighted sum of the two permeabilities ($P^DS \times [U^-]_o/[U_t]_o + P^US \times [UH]_o/[U_t]_o$) was equal to 0.12 $ml \cdot g^{-1} \cdot min^{-1}$, the value of PS_{ecl} estimated in the present study. The solutions are based on an assumed extracellular pH of 7.4, an intracellular pH of 7.0, a dissociation constant for uric acid of 5.0×10^{-6} M ($pK_a = 5.3$), an E_m of −33 mV measured in coronary microvascular endothelial cells from guinea pigs (15), and an extracellular concentration of total uric acid of 40 μM, the normal arterial plasma concentration in guinea pigs (26). In the absence of endothelial uric acid production, $[U_t]_i/[U_t]_o$ equaled 0.40 at low values of P^D/P^U and 0.30 at high values of P^DS/P^US (curve labeled 0). This solution represents the prediction if the assumption of localized endothelial uric acid formation is incorrect. For low values of P^D/P^U, total transport is dominated by the undissociated form of uric acid, the relative concentration, $[UH]/[U_t]$, of which is 2.5-fold higher inside the cell than outside due to lower intracellular pH. For high values of P^DS/P^US, total transport is dominated by the dissociated form of uric acid, the efflux of which is assisted by the negative membrane potential. The neutral undissociated form would not experience the membrane potential. The low range of P^DS/P^US, below ~0.01, is considered the most likely condition, since studies in erythrocytes by Lassen (23) suggest that only the undissociated form of uric acid is transported and the limited lipid solubility of uric acid indicates that membrane PS for the dissociated form of uric acid must be low unless there is a special ionic transporter. In the physiologic range of endothelial uric acid production (1–3 $nmol \cdot g^{-1} \cdot min^{-1}$), intracellular uric acid is predicted to remain below extracellular levels, regardless of which form transported. Only when uric acid production is maximal (7–10 $nmol \cdot g^{-1} \cdot min^{-1}$; Ref. 13) are intracellular concentrations predicted to increase above extracellular levels.

Figure 7 shows the expected effects of different endothelial membrane potentials, E_m, and intracellular pH on the concentration ratio, $[U_t]_i/[U_t]_o$, assuming an extracellular pH of 7.4, a production rate of 3 $nmol \cdot g^{-1} \cdot min^{-1}$, and $[U_t]_o = 40$ μM. In Fig. 7A the effects of E_m are most apparent for high values of P^D/P^U, because only the dissociated form experiences the membrane potential. The intracellular concentration is progressively decreased as the membrane potential is increased from −10 to −80 mV, because the electromotive force assisting efflux is greater. Predictions were also obtained for cardiomyocytes (not shown) using E_m of −80 mV, intracellular pH of 7.0, and PS_{pc}, of 0.01 $ml \cdot g^{-1} \cdot min^{-1}$ If it is assumed that no uric acid is formed in cardiomyoCytes, $[U_t]_i/[U_t]_o$ was equal to 0.4 and 0.05 at the low and high extremes of P^D/P^U, respectively. However, if it was assumed that all uric acid was produced in cardiomyocytes (3 $nmol \cdot g^{-1} \cdot min^{-1}$), then $[U_t]_i/[U_t]_o$ was significantly

elevated, equal to 3.4 and 2.5 at the low and high extremes of P^D/P^U because of the low value for PS_{pc}. The latter prediction is unlikely, based on immunohistochemical evidence showing selective localization of xanthine oxidase/dehydrogenase in capillary endothelial cells in the heart (20).

In Fig. 7B the effects of intracellular pH are most apparent for low values of P^D/P^U, because the relationship between intracellular and extracellular pH may cause large differences in the relative concentrations of the undissociated (transported) form of uric acid on the inside and outside of the membrane. As the intracellular pH is decreased from 7.4 to 6.6, the intracellular concentration is lowered, because progressively less uric acid is dissociated. Figure 7B implies that for intracellular pH of less than ~7.2, uric acid efflux occurs against a concentration gradient, driven by the membrane pH gradient via cotransport of uric acid with H+, if $P^U >> P^D$. These results indicate that any physiological process or experimental intervention that alters intracellular pH or endothelial membrane potential may have a major effect on uric acid transport and on its volume of distribution.

The analysis shown in Figs. 6 and 7 makes it possible to predict the relationship between the steady-state endothelial concentration of uric acid and the value of PS_{ecl}. This relationship is shown in Fig. 8 for three rates of production of uric acid spanning the range reported for coronary endothelial cells in isolated guinea pig hearts (12). For each production rate, two solutions are shown, one for a high and one for a low value of P^D/P^U. The similarity between the pairs of solutions for normal levels of uric acid production (1–3 $nmol \cdot g^{-1} \cdot min^{-1}$) suggests that steady-state concentrations of uric acid are only modestly influenced by the form of uric acid transported (dissociated or undissociated). These results indicate that even if PS_{ecl} is only half the value estimated in the present study, normal endothelial uric acid production (1.5 $nmol \cdot g^{-1} \cdot min^{-1}$) would not be expected to increase endothelial uric acid concentrations above plasma levels. Only under conditions such as ischemia or hypoxia would endothelial uric acid be expected to increase significantly above plasma concentrations. This increase would be blunted if ischemia were accompanied by acidification of endothelial cytoplasm, increasing the concentration of the undissociated form if the ratio $P^D/P^U < 0.01$, as is likely.

The APPENDIX provides general equations for making estimates of the steady-state concentrations of a weak acid or weak base either produced or consumed intracellularly. This is a useful development, given the complexity of the predicted effects of intracellular pH, membrane potential, and the relative importance of the dissociated or undissociated form for membrane transport. The model in its application to uric acid is based on straightforward assumptions: 1) the electrochemical potential for uric acid transport is due entirely to the membrane potential, pH gradient, and concentration gradient of uric acid; 2) transport rates for the dissociated and undissociated forms of uric acid are independent; 3) membrane permeabilities for influx and efflux are the same; 4) the dissociated and undissociated forms of uric acid are in equilibrium both inside and outside the cell; and 5) cellular production of uric acid is independent of concentration. The last assumption would be incorrect if raising the uric acid concentration slowed the xanthine oxidase/dehydrogenase reaction (product inhibition). The analysis does not describe intracellular binding of uric acid; therefore the predictions are for the free solute concentrations.

The present results neither prove nor disprove the existence of a membrane transporter for uric acid on endothelial cells. Evidence in favor of a transporter might be provided by decreasing steady-state endothelial concentrations of uric acid (using allopurinol to block xanthine oxidase/dehydrogenase) but only if the transporter exhibited countertransport inhibition at normal endothelial concentrations of uric acid. There is neither countertransport inhibition nor facilitation with a transporter of the Michaelis-Menten type, where the substrate-transporter complex and the free transporter have equal rates of membrane permeation in the two directions (*cis*-to-*trans* and *trans*-to-*cis*; conformational change). The substrate-transporter complex has a higher permeation rate than the free transporter for the most common type of countertransport, i.e., facilitative. For this type of transporter, allopurinol would tend to reduce PS_{ecl} for uric acid uptake, an effect not readily detectable. Only for the less common inhibitory countertransport, where the free transporter has a higher permeability than the substrate transporter complex, would allopurinol lead to a clearly discernible effect, increased PS_{ecl} for uptake. Therefore experiments using allopurinol are not likely to yield new information.

Acknowledgments

The authors express appreciation for the express technical assistance of James Ploger and Michael Lindholm. The authors also thank Al Ngai for generous help.

This study was supported by National Heart, Lung, and Blood Institute Grant HL-19139.

APPENDIX

Equations were developed to investigate the steady-state cellular concentrations of uric acid by describing the effects of membrane potential, pH gradient, membrane permeability, uric acid dissociation, and cellular production of uric acid. The equations are useful for describing steady-state concentrations of any weak acid. It was assumed that dissociation of uric acid, $UH \rightleftharpoons U^- + H^+$, is in equilibrium with respect to changes in the total concentration, $[U_t]$, which is equal to $[UH] + [U^-]$. Thus the ratio $[U^-]/[UH]$ is determined by the equilibrium expression

$$K_a = \frac{[U^-][H^+]}{[UH]} \quad \text{(A1)}$$

where K_a is the dissociation constant for the weak acid ($pK_a = -\log K_a$). The negative intracellular potential provides a driving force to expel the dissociated form (U^-) of the weak acid, which is not experienced by the neutral undissociated form (UH). Both the dissociated and undissociated forms may permeate the membrane independently.

For the development that follows consider cells bathed in a medium of fixed concentrations, subject to a fixed membrane potential E_m, and producing (or consuming) the weak acid at a fixed rate. The differential equation can be written describing the passive flux of the dissociated form through membrane channels in parallel with the passive flux of the undissociated form across the lipid bilayer itself

$$V\frac{d[U_t]_i}{dt}=S\left\{P^D\left(\left[U^-\right]_o^{'}-\left[U^-\right]_i^{'}\right)+P^U\left([UH]_o-[UH]_i\right)\right\}+Y \quad \text{(A2)}$$

where the subscripts i and o denote intracellular and extracellular concentrations, respectively, V is cell volume (cm^3/g), S is cell surface area (cm^2/g), P^D and P^U are permeabilities (cm/s^{-1}) for the dissociated and undissociated forms, and Y is zero-order production ($mol \cdot g^{-1}.s^{-1}$; a negative Y describes consumption). The primes on [U−]' indicate "apparent concentrations," expressing the electrochemical potential difference across the membrane. The ionic permeability, P^D, will be interpreted as a constant, independent of E_m, and it will be assumed that permeabilities for influx and efflux are equal.

To express Eq. A2 explicitly in terms of E_m, the term $\left[U^-\right]_o^{'}-\left[U^-\right]_i^{'}$ is replaced by an expression based on that used by Goldman (18) in the constant-field equation

$$V\frac{d[U_t]_i}{dt}=S\left\{P^D\frac{E_m zF}{RT}\frac{[U^-]_i e^{E_m zF/RT}-[U^-]_o}{1-e^{E_m zF/RT}}+P^U\left([UH]_o-[UH]_i\right)\right\}+Y \quad \text{(A3)}$$

where E_m, is the membrane potential (inside compared with outside), z is the valence of the ion under consideration (−1 for uric acid), R = 8,314 $A \cdot mV \cdot s \cdot mol^{-1} \cdot {}^{\circ}K^{-1}$, F = 96,480 $A \cdot s \cdot mol^{-1}$, and T = 310°K (37°C). In the absence of a membrane potential (E_m = 0), the net flux of the dissociated form, given by the following term in Eq A3

$$P^D S\frac{E_m zF}{RT}\frac{[U^-]_i e^{E_m zF/RT}-[U^-]_o}{1-e^{E_m zF/RT}}$$

approaches $P^D S([U^-]_o - [U^-]_i)$, rather than zero, since

$$\lim_{x\to 0}\frac{x}{1-e^x}=-1$$

In the steady state, When $d[U_t]_i/dt$ = 0,Eq. A3 may be rewritten

$$P^D S\frac{E_m zF}{RT}\frac{[U^-]_o-[U^-]_i e^{E_m zF/RT}}{1-e^{E_m zF/RT}}=P^U S\left([UH]_o-[UH]_i\right)+Y \quad \text{(A4)}$$

To account for the effect of pH on the degree of dissociation of the weak acid, we make a substitution based on Eq. A1

$$P^D S\frac{E_m zF}{RT}\frac{[U^-]_o-[U^-]_i e^{E_m zF/RT}}{1-e^{E_m zF/RT}}=P^U S\left(\frac{[U^-]_o[H^+]_o}{K_a}-\frac{[U^-]_i[H^+]_i}{K_a}\right)+Y \quad \text{(A5)}$$

$$\frac{P^D S K_a}{P^U S}\frac{E_m zF}{RT}\frac{[U^-]_o-[U^-]_i e^{E_m zF/RT}}{1-e^{E_m zF/RT}}=[U^-]_o\left[H^+\right]_o-[U^-]_i\left[H^+\right]_i+\frac{YK_a}{P^U S} \quad \text{(A6)}$$

For simplicity, let

$$\alpha=\frac{P^{\mathrm{D}}S}{P^{\mathrm{U}}S}\frac{E_{\mathrm{m}}zF}{RT\left(1-e^{E_{m}zF/RT}\right)} \quad \text{(A7)}$$

Then Eq. A6 becomes

$$\left[\mathrm{U}^{-}\right]_{\mathrm{i}}\left[\mathrm{H}^{+}\right]_{\mathrm{i}}-\alpha K_{\mathrm{a}}\left[\mathrm{U}^{-}\right]_{\mathrm{i}}e^{E_{\mathrm{m}}zF/RT}=\left[\mathrm{U}^{-}\right]_{\mathrm{o}}\left[\mathrm{H}^{+}\right]_{\mathrm{o}}-\alpha K_{\mathrm{a}}\left[\mathrm{U}^{-}\right]_{\mathrm{o}}+\frac{YK_{\mathrm{a}}}{P^{\mathrm{U}}S} \quad \text{(A8)}$$

$$\left[\mathrm{U}^{-}\right]_{\mathrm{i}}=\frac{\left[\mathrm{U}^{-}\right]_{\mathrm{o}}\left(\left[\mathrm{H}^{+}\right]_{\mathrm{o}}-\alpha K_{\mathrm{a}}\right)+\frac{YK_{\mathrm{a}}}{P^{\mathrm{U}}S}}{\left[\mathrm{H}^{+}\right]_{\mathrm{i}}-\alpha K_{\mathrm{a}}e^{E_{m}zF/RT}} \quad \text{(A9)}$$

To cast Eq. A9 in terms of the total concentration of the weak acid, we make use of Eq. A1 and the identity, $[U_t] = [U^-] + [UH]$, to write

$$\left[\mathrm{U}^{-}\right]=\frac{\left[\mathrm{U}_{\mathrm{t}}\right]K_{\mathrm{a}}}{K_{\mathrm{a}}+\left[\mathrm{H}^{+}\right]} \quad \text{(A10)}$$

This result was substituted into Eq. A9, which after rearrangement leads to

$$\left[\mathrm{U}_{\mathrm{t}}\right]_{\mathrm{i}}=\frac{\left(K_{\mathrm{a}}+\left[\mathrm{H}^{+}\right]_{\mathrm{i}}\right)\left(\frac{\left[\mathrm{U}_{\mathrm{t}}\right]_{\mathrm{o}}K_{\mathrm{a}}}{K_{\mathrm{a}}+\left[\mathrm{H}^{+}\right]_{\mathrm{o}}}\left(\left[\mathrm{H}^{+}\right]_{\mathrm{o}}-\alpha K_{\mathrm{a}}\right)+\frac{YK_{\mathrm{a}}}{P^{\mathrm{U}}S}\right)}{K_{\mathrm{a}}\left(\left[\mathrm{H}^{+}\right]_{\mathrm{i}}-\alpha K_{\mathrm{a}}e^{E_{m}zF/RT}\right)} \quad \text{(A11)}$$

The units of Eq.A11, $[U_t]_i$ = mol/cm^3, are confirmed by

$$\frac{\left(mol/cm^{3}+mol/cm^{3}\right)\left[\frac{mol/cm^{3}\times mol/cm^{3}}{mol/cm^{3}+mol/cm^{3}}\left(mol/cm^{3}-mol/cm^{3}\right)+\frac{mol\cdot s^{-1}\cdot g^{-1}\times mol/cm^{3}}{cm^{3}\cdot s^{-1}\cdot g^{-1}}\right]}{mol/cm^{3}\left(mol/cm^{3}-mol/cm^{3}\right)}$$

after noting that α and $e^{E_m zF/RT}$ are dimensionless.

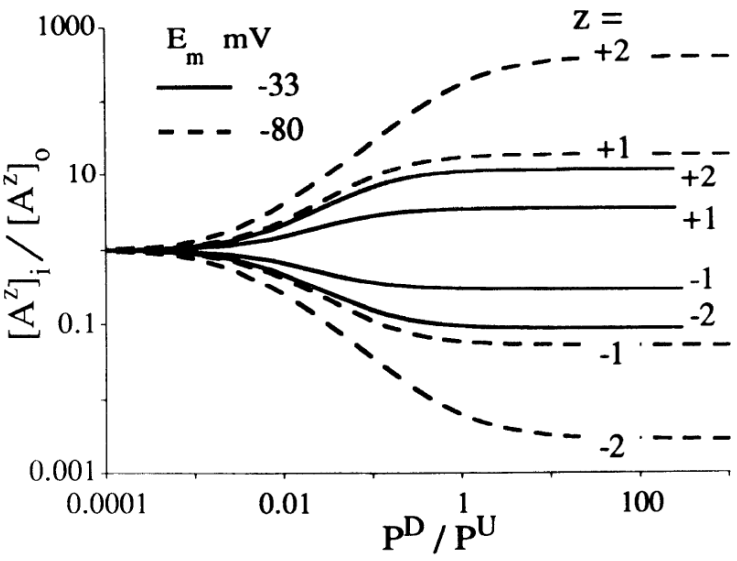

Fig. 9.

Predicted effect of ionic valence (*Z*) on steady-state cellular concentrations of a partially dissociated species. Ordinate, $[A^Z]_i/[A^Z]_0$, is ratio of intracellular to extracellular concentrations of dissociated plus undissociated forms calculated using *Eq. A11*. Abscissa, P^D/P^U, is ratio of membrane permeabilities for dissociated to undissociated forms of species, where concentration-weighted sum of permeabilities ($P^DS \times [U^-]_o/[U_t]_0 + P^US \times [UH]_o/[U_t]_0$ is constant. Solutions were obtained for 4 values of *Z* at each of 2 values of membrane potential E_m, where $[H^+]_i = [H^+]_0$ to eliminate acid-base influences and Y = 0 to model equilibrium conditions. Inflection point of curves occurs at (P^DK_w) = 1, where K_a, is dissociation constant of the water (10^{-7}M).

In the absence of any permeability for the dissociated form, i.e., $P^D = 0$, then $\alpha = 0$, and Eq. A11 becomes

$$[U_t]_i = \frac{(K_a + [H^+]_i)\left(\frac{[U_t]_o K_a [H^+]_o}{K_a [H^+]_o} + \frac{Y K_a}{P^U S}\right)}{K_a [H^+]_i} \quad \text{(A12)}$$

When both intracellular and extracellular pH equal pK_a, this expression reduces to

$$[U_t]_i = [U_t]_o + \frac{2Y}{P^U S} \quad \text{(A13)}$$

where the effective permeability is $P^US/2$, since the anion is half-dissociated. When ionization is totally suppressed, i.e., $[H^+]_i$ and $[H^+]_o \gg K_a$, then

$$[U_t]_i = [U_t]_o + \frac{Y}{P^U S} \quad \text{(A14)}$$

as for any nonionizing species, produced inside the cell.

At the opposite extreme, when ionization is complete, i.e., $[U^-] \gg [UH]$, then from Eg. A4, with $x = E_m zF/RT$ and $P^D S \neq 0$

$$[U_t]_i = e^x \left\{ [U_t]_o - \frac{(1 - e^x) Y}{x P^D S} \right\} \quad \text{(A15)}$$

When E_m or $x \to 0$, $(1 - e^x)/x \to -1$, then Eq. A15 reduces to

$$[U_t]_i = [U_t]_o + \frac{U}{P^D S} \quad \text{(A16)}$$

which is analogous to Eq. A14.

The ratio of the intracellular virtual volume of distribution (V_i') to the real volume of water in the cell (V_i) in which the solute is dissolved can be determined from the concentration ratio, given in the steady state by

$$\frac{V_i'}{V_i} = \frac{[U_t]_i}{[U_t]_o} \quad \text{(A17)}$$

Equation A11 can be used to describe the steady-state behavior of partially dissociated monovalent and divalent cations and anions by choosing appropriate values for z. Solutions for Eq. A11, shown in Fig. 9, were obtained for z of −2, −1, +l, and +2, for E_m of −33 and −80 mV, and pH_i equal to pH_o. In this case, K_a is the dissociation constant for the cation or anion rather than a weak acid. These results show that a divalent anion is more effectively excluded from the cell than a monovalent anion and that a divalent cation is more effectively concentrated inside the cell than a monovalent cation. These effects are only significant when the permeability for the ionized form, P^D, is relatively large.

The relative magnitudes of the unidirectional influx rates of the dissociated (J^D) and undissociated (J^U) forms may be assessed by noting that these quantities are implicit in Eq. A3

$$J^D = -P^D S \times \frac{E_m zF}{RT} \frac{[U^-]_o}{1 - e^{E_m zF/RT}} = \alpha P^U S [U^-]_o \quad \text{(A18)}$$

$$J^U = P^U S \times [UH]_o \quad \text{(A19)}$$

It was assumed that $P^U S = 100 \times P^D S$, E_m is −33 mV, z is −1, and pH_o is 7.4, in which case $[U-]_o/[UH]_o$ is 126. Dividing Eq. A18 by A19

$$\frac{J_D}{J_U} = \alpha \frac{[U^-]_o}{[UH]_o} = -\frac{E_m zF}{RT} \frac{1}{1 - e^{E_m zF/RT}} \times \frac{126}{100} = 0.63 \quad \text{(A20)}$$

The analysis presented above does not account for the activities of solutes, the dependence of K_a on temperature and ionic strength, nor intracellular binding of the weak acid.

REFERENCES

1. Anversa P, Levicky V, Beghi C, McDonald SL, Kikkawa Y. Morphometry of exercise-induced right ventricular hypertrophy in the rat. Circ. Res. 1983; 52:57–64. [PubMed: 6848210]
2. Bardenheuer H, Schrader J. Supply-to-demand ratio for oxygen determines formation of adenosine by the heart. Am. J. Physiol. 1986; 250:H173–H180. (Heart Circ. Physiol. 19). [PubMed: 3004232]
3. Bassingthwaighte JB. Plasma indicator dispersion in arteries of the human leg. Circ. Res. 1966; 19:332–346. [PubMed: 5330717]
4. Bassingthwaighte JB, Chaloupka M. Sensitivity functions in the estimation of parameters of cellular exchange. Federation Proc. 1984; 43:180–184.
5. Bassingthwaighte, JB.; Goresky, CA. Handbook of Physiology. The Cardiovascular System. Microcirculation. Vol. IV. Am. Physiol. Soc.; Bethesda, MD: 1984. Modeling in the analysis of solute and water exchange in the microvasculature; p. 549-626.sect. 2chapt. 13
6. Bassingthwaighte JB, King RB, Roger SA. Fractal nature of regional myocardial blood flow heterogeneity. Circ. Res. 1989; 65:578–590. [PubMed: 2766485]
7. Bassingthwaighte JB, Knopp TF, Anderson DU. Flow estimation by indicator dilution (bolus injection): reduction of errors due to time-averaged sampling during unsteady flow. Circ. Res. 1970; 27:277–291. [PubMed: 4917088]
8. Bassingthwaighte JB, Sparks HV. Indicator dilution estimation of capillary endothelial transport. Annu. Rev. Physiol. 1986; 48:321–334. [PubMed: 3518617]
9. Bassingthwaighte JB, van Beek JHGM, King RB. Fractal branchings: the basis of myocardial flow hetero geneities? Ann. NY Acad. Sci. 1990; 591:392–401. [PubMed: 2197931]
10. Bassingthwaighte JB, Wang CY, Chan IS. Blood-tissue exchange via transport and transformation by endothelial cells. Circ. Res. 1989; 65:997–1020. [PubMed: 2791233]
11. Bassingthwaighte JB, Yipintsoi T, Harvey RB. Microvasculature of the dog left ventricular myocardium. Microvasc. Res. 1974; 7:229–249. [PubMed: 4596001]
12. Becker, BF.; Gerlach, E.; Becker, BF. Uric acid, the major catabolite of cardiac adenine nucleotides and adenosine, originates in the coronary endothelium. In: Gerlach, E., editor. Topics and Perspectives in Adenosine Research. Springer-Verlag; Berlin: 1987. p. 209-222.
13. Becker BF, Reinholz N, Ozcelik T, Leipert B, Gerlach E. Uric acid as radical scavenger and antioxidant in the heart. Pfluegers Arch. 1989; 415:127–135. [PubMed: 2556684]
14. Catravas, JD.; Bassingthwaighte, JB.; Sparks, HV, Jr.. Adenosine transport and uptake by cardiac and pulmonary endothelial cells. In: Ryan, US., editor. Endothelial Cells. Vol. I. CRC; Boca Raton, FL: 1988. p. 65-84.chapt. 5
15. Daut J, Mehrke G, Nees S, Newman WH. Passive electrical properties and electrogenic sodium transport of cultured guinea-pig coronary endothelial cells. J. Physiol. Lond. 1988; 402:237–254. [PubMed: 2853223]
16. Escribano J, Garcia-Canovas F, Garcia-Carmona F. A kinetic study of hypoxanthine oxidation by milk xanthine oxidase. Biochem. J. 1988; 254:829–833. [PubMed: 3196295]
17. Florkin M, Duchateau G. Les formes du système enzymatique de l‘uricolyse et l‘évolution du catabolisme purique chez les animaux. Arch. Int. Physiol. 1943; 53:267–307.
18. Goldman DE. Potential, impedance, and rectification in membranes. J. Gen. Physiol. 1943; 27:37–60. [PubMed: 19873371]
19. Gorman MW, Wangler RD, Sparks HV. Distribution of perfusate flow during vasodilation in the isolated guinea pig heart. Am. J. Physiol. 1989; 256:H297–H301. (Heart Circ. Physiol. 25). [PubMed: 2912192]
20. Jarasch ED, Bruder G, Heid HW. Significance of xanthine oxidase in capillary endothelial cells. Acta Physiol. Scand. 1986; 548(Suppl):39–46.
21. King RB, Bassingthwaighte JB, Hales JRS, Rowell LB. Stability of heterogeneity of myocardial blood flow in normal awake baboons. Circ. Res. 1985; 57:285–295. [PubMed: 4017198]
22. Kuikka J, Levin M, Bassingthwaighte JB. Multiple tracer dilution estimates of d- and 2-deoxy-d-glucose uptake by the heart. Am. J. Physiol. 1986; 250:H29–H42. (Heart Circ. Physiol. 19). [PubMed: 3510568]

23. Lassen UV. Kinetics of uric acid transport in human erythrocytes. Biochim. Biophys. Acta. 1961; 53:557–569. [PubMed: 14462629]
24. LeFevre PG, Marshall JK. Conformational specificity in a biological sugar transport system. Am. J. Physiol. 1958; 194:333–337. [PubMed: 13559473]
25. McConahey PJ, Dixon FJ. A method of trace iodination of proteins for immunologic studies. Int. Arch. Allergy. 1966; 29:185–189. [PubMed: 4160044]
26. Mudge GH, McAlary B, Berndt W0. Renal transport of uric acid in the guinea pig. Am. J. Physiol. 1968; 214:875–879. [PubMed: 5642951]
27. Nees S, Herzog V, Becker BF, Böck M, Rosiers C. Des, Gerlach E. The coronary endothelium: a highly active metabolic barrier for adenosine. Basic Res. Cardiol. 1985; 80:515–529. [PubMed: 3000345]
28. Rose CP, Goresky CA. Vasomotor control of capillary transit time heterogeneity in the canine coronary circulation. Circ. Res. 1976; 39:541–554. [PubMed: 786495]
29. Schafer DE, Johnson JA. Permeability of mammalian heart capillaries to sucrose and inulin. Am. J. Physiol. 1964; 206:985–991. [PubMed: 14208975]
30. Stein, WD. Transport and Diffusion Across Cell Membranes. Academic; Orlando, FL: 1986.
31. Wangler RD, Gorman MW, Wang CY, Dewitt DF, Chan IS, Bassingthwaighte JB, Sparks HV. Transcapillary adenosine transport and interstitial adenosine concentration in guinea pig hearts. Am. J. Physiol. 1989; 257:H89–H106. (Heart Circ. Phvsiol. 26). [PubMed: 2750952]

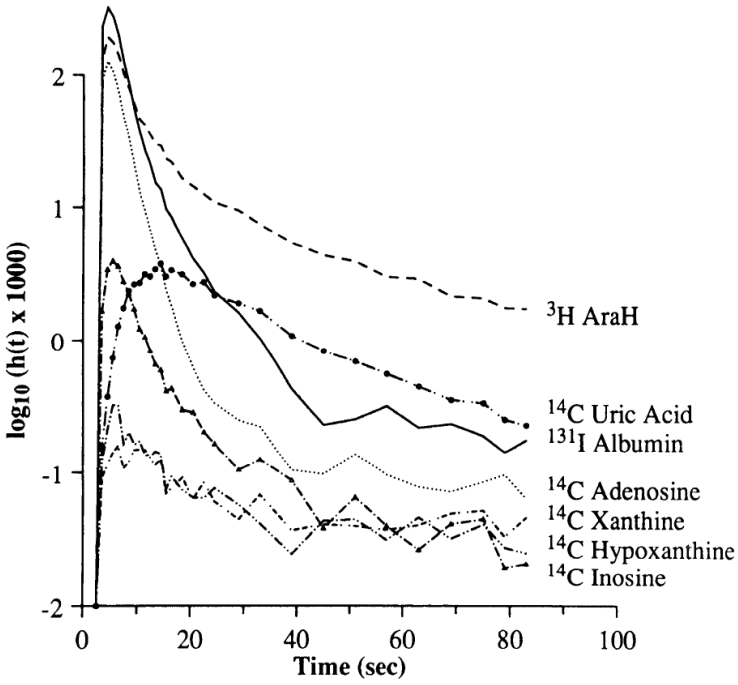

Fig. 1.

Multiple indicator-dilution results obtained by intracoronary injection of tracer adenosine [and reference tracers, 9-β-D-arabinofuranosyl hypoxanthine (AraH) and albumin] and analysis of coronary outflow concentrations of injected tracers and labeled metabolites, inosine, hypoxanthine, xanthine, and uric acid, in an isolated guinea pig heart (*2502882*). Adenosine metabolites are irreversibly produced by sequence of enzymes, adenosine deaminase, purine nucleoside phosphorylase, and xanthine oxidase/dehydrogenase. Inosine emerged with nearly same time course as precursor adenosine, and outflow concentrations of hypoxanthine and xanthine were low. In contrast, outflow of uric acid was greater than inosine, and there was a marked delay in efflux.

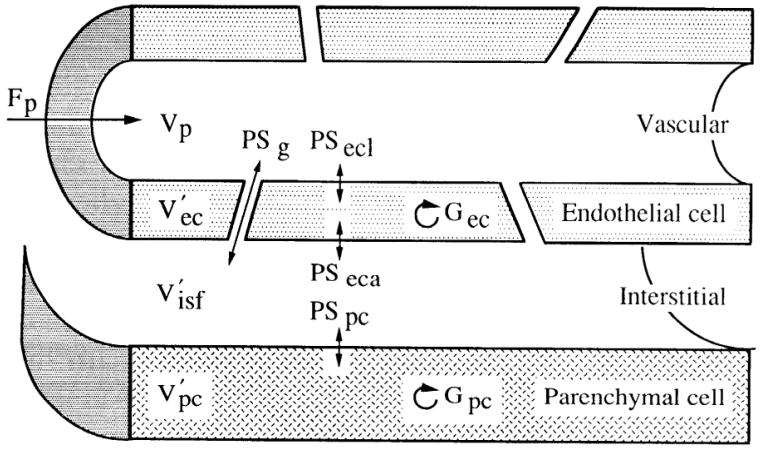

Fig. 2.

Structure of capaillary exchange unit in axially distributed capillary-tissue model used in analysis (see METHODS, Model parameters for definitions of symbols). Each exchange unit consisted of 4 regions, vascular, endothelial, interstitial, and parenchymal. Because PS_{pc} was constrained to 0, parenchymal region played no role in modeling of uric acid. Each exchange unit was also associated in series with a dispersive nonexchanging large vessel unit. Complete model comprised 20 parallel capillary pathways, identical except for their flow, F_p, which was distributed among pathways, to account for effects of regional flow heterogeneity (see METHODS). In model, albumin was restricted to vascular region, L-glucose to extracellular region, and uric acid was free to enter endothelial region.

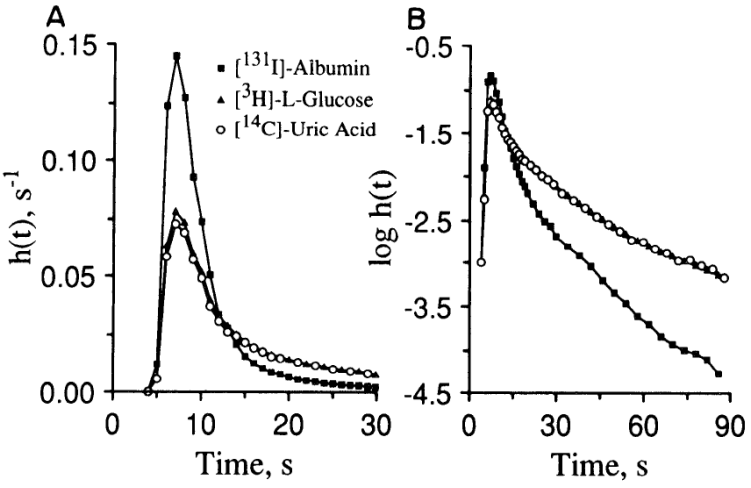

Fig. 3.

Uric acid multiple indictor-dilution curves odtained in 1 of triple-label studies in an isolated guinea pig heart (*expt no. 21098911*). Heart was perfused with normal medium at a flow rate of 2.4 $ml \cdot g^{-1} \cdot min^{-1}$ and a pressure of 55 mmHg. Fraction of injected tracer emerging in coronary outflow per second, *h(t)*, is shown. *A*: early portion of curve, using a linear scale for *h(t)*, for clarity of curve peak. *B*: log *h(t)* for entire curve. Beginning at 20 s, alternating uric acid and L-glucose data points have been omitted, so that similarity of late portions of both curves can be noted. Lines connecting symbols do not represent model solutions.

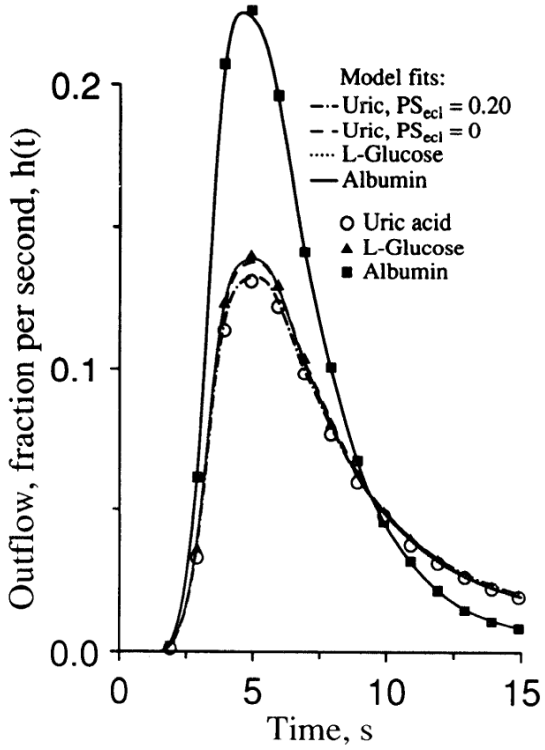

Fig. 4.

Model fits to uric acid dilution curve from triple-label studies (*expt no. 21098921*). Model solutions for albumin, L-glucose, and uric acid are shown by continuous curves; tracer dilution measurements by symbols. Two uric acid solutions are shown, one assuming no endothelial membrane permeability ($PS_{ecl} = 0$), which is very similar to the Lglucose solution, and one assuming $PS_{ecl} = 0.20$ ml·g^{-1}·min^{-1}, which passes through uric acid data. All other model parameter values were identical for both uric acid solutions. Uric acid solutions account for difference in molecular weights between uric acid and L-glucose. Only peak of curve is shown; at later times, difference between uric acid solutions was smaller. Heart was perfused with normal medium at a flow rate of 3.5 ml·g^{-1}·min^{-1} and a pressure of 65 mmHg.

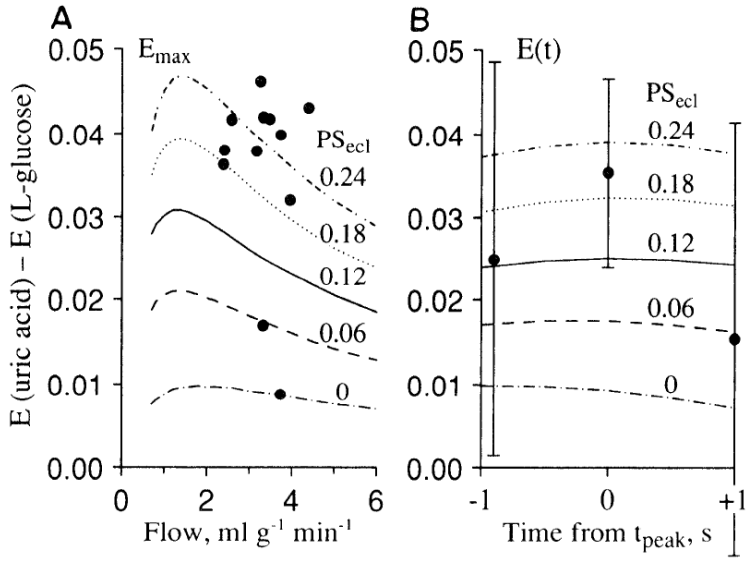

Fig. 5.

Excess extraction of uric acid over L-glucose; dependence on coronary flow (*A*) and time course (*B*). Model solutions are shown by continuous curves for 5 values of PS_{ecl}; outflow measurements from triple-label studies are shown by symbols. *A*: model solutions represent difference between peak extractions, E_{max} for uric acid and L-glucose over the flow range indicated. Model parameter values were taken from a representative experiment, except PS_{ecl}, which was varied as indicated. Individual measurements are from 12 experiments. *B*: time courses of identical model solutions are shown together with outflow measurements (means ± SD, n = l2), for 3 s at peak of curve. Time axis is shown relative to peak of each curve, t_{peak}. For model solutions, flow was 3.3 ml·g^{-1} min^{-1} average value in triple-label studies.

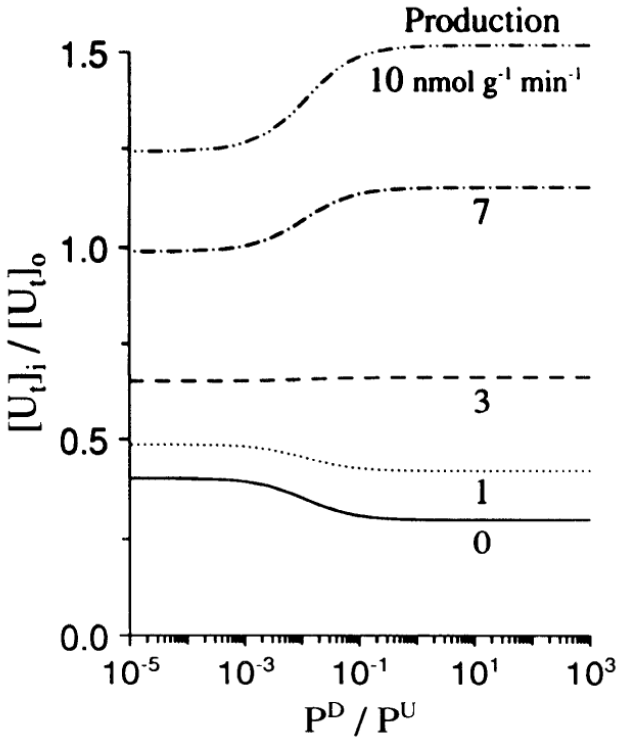

Fig. 6.

Predicated effect of uric acid prodution on steady-state endothelial concentrations of uric acid. Curves were obtained by solving Eq. A11 in APPENDIX for 5 values of production; $[U_t]_0$ = 40 μM, pH_0 = 7.4, pH_i = 7.0, pK_a = 5.3, E_m, = −33 mV, z = −1, and $P^DS \times [U^-]_0/[U_t]_0 + P^US \times [UH]_0/[U_t]_0$ = 0.12 ml·g^{-1}·min^{-1}.

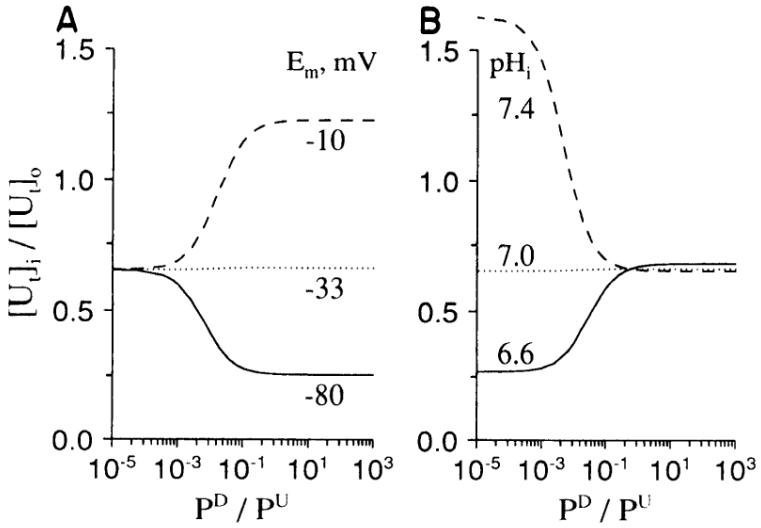

Fig. 7.

Predicted effects of membrane potential (*A*) and intracellular pH (*B*) on steady-state endothelial concentrations of uric acid. Curves were obtained using Eq. A11 for 3 values of E_m (*A*) and for 3 values of pHi (*B*); production was equal to 3 nmol·g^{-1}·min^{-1} and other parameters had values given in legend to Fig. 6.

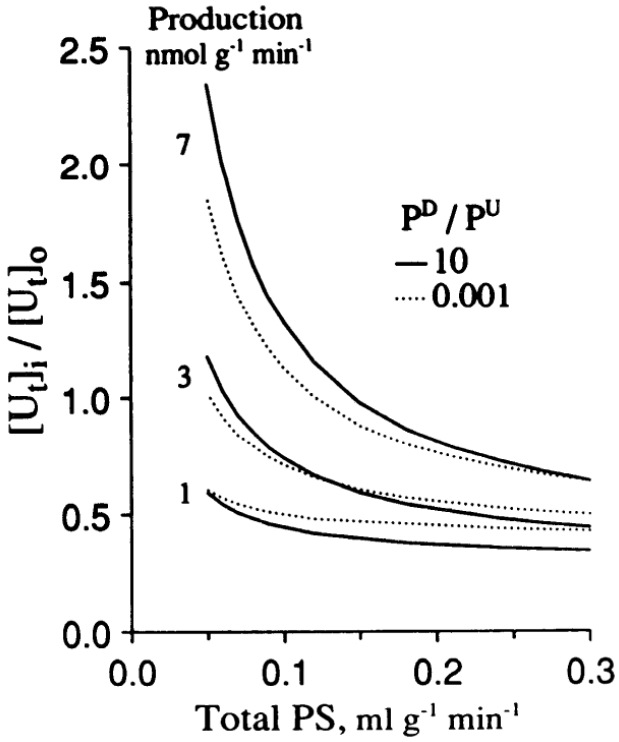

Fig. 8.

Predicted relationship between value of total endothelial membrane *PS* (PS_{ecl} and steady-state endothelial concentrations of uric acid. Curves were obtained using Eq. A11 for 3 values of endothelial uric acid production; other parameters had values given in legend to Fig. 6. For each value of production, 2 curves are shown, one for a high value of P^D/P^U (solid line) and one for a low value of P^D/P^U (dottedline).

Table 1

Coronary flow and peak relative extractions of tracer L-glucose and uric acid in triple-label studies in the guinea pig heart

Expt No.	Flow, $ml \cdot g^{-1} \cdot min^{-1}$	E_{max}	
		L-Glucose	Uric acid
21098911	2.4	0.460	0.496
21098912	2.6	0.375	0.417
21098913	2.4	0.412	0.450
21098921	3.5	0.382	0.423
21098922	3.3	0.367	0.413
21098923	3.2	0.404	0.442
16118911	4.4	0.383	0.426
16118912	3.7	0.383	0.392
16118913	3.7	0.381	0.421
16118921	3.3	0.358	0.375
16118922	3.3	0.376	0.418
16118923	3.9	0.328	0.360
Mean ± SD	3.3±0.6	0.384±O.032	0.419±0.035

E_{max} is relative extraction, E(*t*), of the diffusible tracers, L-glucose and uric acid, compared with intravascular reference, albumin, determined at peak of dilution curves (see METHODS, *Calculation of Dilution Curves*). $P < 0.005$ for difference between peak extractions (paired *t* test).

Table 2

Values of model parameters describing extracellular transport optimized to fit L-glucose curves for triple-label group

Expt No.	PS_g, ml·g^{-1}·min^{-1}	V'_{isf}, ml/g	CV, %
21098911	2.35	0.328	16.1
21098912	1.84	0.300	7.28
21098913	1.68	0.367	10.1
21098921	2.48	0.413	5.34
21098922	2.24	0.368	5.89
21098923	2.41	0.412	4.38
16118911	2.79	0.295	4.96
16118912	2.60	0.450	13.9
16118913	2.66	0.349	9.88
16118921	2.30	0.260	9.65
16118922	2.41	0.383	8.92
16118923	2.42	0.313	5.55
Mean ± SD	2.35±0.32	0.353±0.056	8.50±3.69

PS_g, permeability-surface area product for extracellular transport between vascular and interstitial region; V'_{isf}, volume of distribution in interstitial region; CV, coefficient of variation (SD/mean) of model fit to measured dilution curves. In experiments ending in *1* or *3*, perfusion medium contained no uric acid; in experiments ending in *2*, it contained 1 mM uric acid.

Table 3

Model estimates of endothelial cell membrane permeability for uric acid and the coefficients of variation of model fits

Expt No.	PS_{ecl} (Optimized), $ml \cdot g^{-1} min^{\cdot -1}$	CV, %, Obtained Using PS_{ecl} =			
		Optimized	0	0.2	0.3
Triple-label studies					
21098911	0.18	16.6	20.2	16.6	17.0
21098912	0.19	8.16	11.4	8.29	9.46
21098913	0.17	8.78	11.8	8.80	9.75
21098921	0.20	7.35	9.47	7.35	7.86
21098922	0.20	7.08	10.2	7.08	7.51
21098923	0.16	7.12	8.67	7.74	9.61
16118911	0	13.6	13.6	14.6	15.2
16118912	0	17.4	17.4	21.9	23.0
16118913	0.13	10.1	10.7	10.8	12.2
16118921	0	14.6	14.6	19.0	20.5
16118922	0	12.7	12.7	15.7	16.9
16118923	0.18	5.13	7.87	5.16	6.05
Mean ± SD	0.12±0.09	10.7±4.11	12.4±13.62	11.9±5.43	12.9±5.50
Dual-label studies					
13128911	0.047	6.74	6.83	7.76	8.92
13128912	0	5.90	5.90	8.15	9.30
13128913	0.070	7.75	7.88	7.93	8.45
13128921	0.080	12.1	11.9	12.2	12.3
13128922	0.076	9.28	9.40	9.51	9.91
13128923	0.032	6.63	6.68	8.19	9.54
Mean ± SD	0.051±O.O31	8.07±2.30	8.10±2.2	8.96±1.71	9.74±1.35

$P < 0.005$ for difference between coefficients of variation (CV) obtained using optimized values of endothelial cell membrane perme ability (PS_{ecl}) and values of 0, 0.2, and 0.3 $ml \cdot g^{-1} \cdot min^{-1}$, based on pooled triple- and dual-label studies ($n = 18$, paired t test). In experiments ending in *1* or *3*, perfusion medium contained no uric acid; in experiments ending in *2*, it contained 1 mM uric acid.